
Proceedings Paper:
Basheer, M orcid.org/0000-0002-0835-8029, Yang, K, Ma, Q et al. (3 more authors) (2018) Comparison of chloride-induced corrosion between alkali-activated slag concretes and Portland cement concretes. In: Proceedings of the 3rd R. N. Raikar Memorial International Conference & Gettu-Kodur International Symposium on Advances in Science & Technology of Concrete. 3rd R N Raikar Memorial International Conference & Gettu-Kodur International Symposium on Advances in Science & Technology of Concrete, 14-15 Dec 2018, Mumbai, India. India Chapter of American Concrete Institute .

Comparison of chloride-induced corrosion between alkali-activated slag concretes and Portland cement concretes

Muhammed Basheer, Kai Yang
School of Civil Engineering, University of Leeds, UK

Qianmin Ma
Department of Civil Engineering, University of Kunming University of Science and Technology, China

Sreejith Nanukuttan
School of Natural and Built Environment, Queen's University Belfast, UK

Changhui Yang
College of Materials Science and Engineering, Chongqing University, China

Yun Bai
Civil, Environmental and Geomatic Engineering, University College London, UK

ABSTRACT

It is reported that the diffusion of chlorides in Alkali-activated slag (AAS) concretes is lower than that in Portland cement (PC) counterparts and is comparable to concretes containing high volumes of supplementary cementitious materials. This is considered to be due to its dense calcium silicate hydrate structure and relatively better chloride binding capacity due to its high alumina content. However, a critical review of the literature indicated that both the resistance to chloride ingress and chloride-induced corrosion of steel in AAS concretes are not found uniformly in all publications. Further, less is known about the effect of mix proportions, including binder content, water-binder ratio, role of activator, etc. on the rate of chloride transport through AAS concretes. As a consequence, there is conflicting information on the ability of AAS concretes to delay both the onset and the rate of corrosion of embedded steel in such concretes. Therefore, a thorough investigation was carried out focusing on their permeation properties and the corrosion behaviour in them. The results obtained from this research has illustrated that AAS concretes could achieve lower non-steady state diffusion coefficient and higher degree of chloride binding, resulting in improved corrosion resistance. However, there is a need to optimise mix proportions as there was a significant influence and interaction between both Na_2O % and Ms of water glass used as activator for the AAS binder.

Keywords: AAS, corrosion, chloride transport, pore solution chemistry, mix proportions

INTRODUCTION

Alkali-activated slag (AAS) is a clinker-free binder with dense calcium silicate hydrate structure. As a result, it offers the possibility of achieving desirable mechanical properties that are comparable to those of Portland cement (PC) concretes, whilst ensuring significant reductions in greenhouse gas emissions [1, 2]. Due to its high alumina content, it has the potential for high chloride binding capacity [3]. Numerous studies have been carried out to examine the durability performance of AAS [3-8]. Most of them have focused on determining the pore structure characteristics [4, 6], transport properties such as gas, water and chloride transport [3, 4], whereas relatively little has been reported on the corrosion of reinforcing steel in AAS concretes [6-8], despite corrosion is the main cause of premature degradation of reinforced concrete structures in severe environments. Unlike the PC system, the AAS consists of a binder that is made up of slag and an activator, most common one is sodium silicate (water glass - WG) solution. The activator composition is commonly expressed in two parts, silicate modulus (Ms) and alkali concentration (expressed as Na_2O%). The exact effect of these compositions on chloride transport and/or subsequent corrosion is also unclear. A review of literature since 1980's has indicated that in some cases the chloride diffusion in AAS concrete is lower than the Portland cement (PC) counterparts and is comparable to concretes containing high volumes of supplementary cementitious materials [3], but this has not been found in all cases [2, 7]. It is recognised that the passivity of reinforcing steel in concrete, whether based on PC or AAS, is attributed to the formation of a thin passive film on the steel surface [7, 9]. This film is maintained by the high pH of the surrounding concrete, unless the film

is damaged by the presence of chloride ions or by a pH drop due to carbonation of the concrete [2, 5, 7-9]. That is, both the transport properties and pore solution characteristics will affect the corrosion behaviour of steel in AAS. Given the differences in raw materials and the hydration/polymerisation process between AAS and PC, the initiation and propagation of corrosion are expected to be different [7]. Therefore, it is important to establish whether or not AAS concretes could be used for reinforced concrete structures in chloride exposure environments [10].

Therefore, a programme of investigation was carried out with the objectives of studying: (i) the chloride transport in various AAS concretes; (ii) the physical and chemical characteristics of the pore structure and the pore solution; and (iii) corrosion of embedded steel when these concretes were exposed to an intermittent chloride ponding environment. In this paper, the results from this investigation are presented and discussed so as to understand the suitability and limitations, if any, of AAS concretes for chloride exposure environments, particularly where chloride-induced corrosion is a potential risk for the premature deterioration of reinforced concrete structures.

RESEARCH METHODOLOGY

BS EN 206-1 [10] suggests different strength classes for the different chloride exposure environments. Accordingly, for exposure classes XS2, XS3 and XD3, the strength class recommended is C45. Therefore, the target strength class of the AAS concretes in this research was C45. The selected slump class was S2, i.e. the target slump was 40-90mm.

Materials and Mix Proportions

All the AAS concretes were manufactured by activating ground granulated blast-furnace slag (GGBS) conforming to BS EN 15167-1:2006 [11], which was supplied by Civil and Marine Ltd., UK. Sodium silicate solution (WG) with an initial Na_2O% of 12.45 and SiO_2% of 43.60 was used to make up the activator. Industrial grade sodium hydroxide powder with a purity of 99 % was used to adjust the composition of the WG solution to required silica modulus and alkali concentration. To control the setting time of the AAS concretes a barium based retarder 'YP-1' [12] was used. It was dry-blended with GGBS before mixing. The PC concrete was manufactured with Class 42.5 N PC (CEM-I) conforming to BS EN 197-1: 2000 [13]. A polycarboxylic polymer based superplasticiser with a water content of 40% was used in the PC concrete mix. The extra water in the superplasticizer was accounted for whilst determining the mixing water content. Crushed basalt from Northern Ireland with size fractions of 20mm and 10mm combined in a ratio of 1:1 was used as the coarse aggregate. Natural sand with fineness modulus of 2.53 was used as the fine aggregate.

The various mix proportions of concretes investigated in this research are summarized in Table 1. Altogether there were 12 AAS concretes mixes, which were manufactured with Na_2O% of 4, 6, and 8 and Ms of WG of 0.75, 1.00, 1.50 and 2.00. The PC concrete mix was manufactured with the total binder content same as that of the AAS concretes. The water to binder ratio (w/b) of the AAS concretes was 0.47, as compared to 0.42 used for the PC mix. The higher water to binder ratio for AAS was essential to ensure that the mixes were workable and majority of the mixes resulted in a slump between 40 and 90 mm.

Table 1. Mix proportions of concretes

Mix NO (Na2O-MS)	Na2O (%)	Ms	Binder (kg/m^3)	Sodium silicate (kg/m^3)	NaOH (kg/m^3)	Retarder (kg/m^3)	Fine aggregate (kg/m^3)	Coarse aggregate (kg/m^3)
4%-0.75	4	0.75	371	34.6	13.6	1.11	654	1163
4%-1.00	4	1.00	368	45.8	11.6	1.10	655	1164
4%-1.50	4	1.50	362	67.7	7.8	1.08	656	1167
4%-2.00	4	2.00	357	88.9	4.2	1.07	658	1170
6%-0.75	6	0.75	358	19.7	19.7	1.07	654	1163
6%-1.00	6	1.00	354	16.8	16.8	1.08	655	1165
6%-1.50	6	1.50	346	11.2	11.2	1.06	658	1169
6%-2.00	6	2.00	339	5.9	5.9	1.04	660	1173
8%-0.75	8	0.75	346	25.4	25.4	1.02	654	1163
8%-1.00	8	1.00	341	21.6	21.6	1.04	656	1166
8%-1.50	8	1.50	332	14.3	14.3	1.02	658	1171
8%-2.00	8	2.00	322	7.5	7.5	0.97	661	1175
PC	-	-	-	-	-		686	1220

Note: Cement content for PC was 400 kg/m3 and superplasticiser dosage was 0.5 % by mass of cement.

Test Specimens

Six 250x250x110mm concrete blocks were cast, of which three had embedded steel bars whilst the other three had no steel. Nine 100mm size concrete cubes were also cast for carrying out the strength test. Figure 1 shows the schematic representation of the concrete block with embedded steel bars, one of which at the top acts as the anode and the other three bars at the bottom act as the cathode. Before embedding the steel bars, they were cleaned first with a wire brush and then with a dry cleaning cloth to remove any rust and debris, at which stage they were weighed. Also shown in this figure are the location of sheathed stainless steel bars with a limited opening towards the middle of the sample so that it can act as a sensor. They are hereafter referred to as electrodes and were used for measuring the electrical resistivity of the concretes during the cycling ponding/drying regime.

Both the blocks and the cubes were cast by following the procedure given in BS 1881-125:1986 [14]. After casting the test specimens, they were covered with thick polythene sheets to minimise evaporation of water from the surface of concrete. Approximately 1h after the concrete surface became stiff, the moulds were covered with a layer of previously wetted hessian and then covered with a layer of polythene sheet. The samples were stored for 3 days and then the specimens were demoulded, wrapped in wet hessian and plastic bags, and stored in a constant temperature room kept at 20 (± 1)^{o}C for 91 days. The hessian was checked for its moisture condition at every 2 weeks and rewetted if needed.

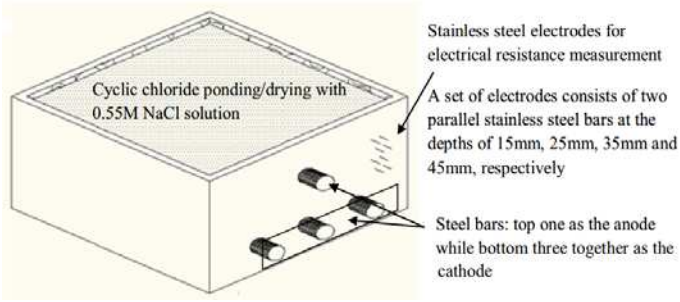

Figure 1. Schematic representation of the concrete block used for the corrosion tests with a dyke in the middle for ponding chloride solution

Test Methods

Slump and Compressive Strength

The slump of the fresh concrete was measured by following the procedure in BS EN 12350-2:2009 [15] and the compressive strength was determined using 100mm cubes at the age of 3, 28 and 91 days in accordance with the procedure in BS EN 12390-3:2009 [16].

Chloride Diffusivity

The chloride transport was determined by carrying out a non-steady state chloride diffusion test in accordance with NT BUILD 443 [17]. After 90 days of storage, three cores of 100mm diameter per mix were cored from the 250x250x110 mm concrete blocks. A slice with a thickness of 50mm from the casting surface (trowel finished face) was cut off and the rest was kept for carrying out the test. The vacuum saturation regime similar to that of NT BUILD 492 [18] was used to precondition the cores, as this takes approximately 18 hours, the test age of samples was 91days. Before the non-steady state chloride diffusion test, the bulk electrical resistivity of the cores was determined by using a method described in the Chlortest report [19], which is considered to indicate the pore structure of the concrete.

Corrosion of the Embedded Steel Bars

One month before the test age of 91 days, the three concrete blocks with the embedded steel bars and electrodes were moved to a controlled environment (temperature: 23± 3^{o}C, RH: 55±10%) and kept there for a duration of 2 weeks. An epoxy resin was applied onto four side surfaces. The blocks were then stored at the above condition for another 2 weeks. Approximately 200ml of NaCl solution with the concentration of 0.55M was used to pond the blocks for 1day followed by 6 days for drying. This cycle of intermittent chloride intermittent ponding was continued until the end of the test (250+ days). During the whole conditioning and testing periods, the blocks were supported by two timber strips to allow air flow under the blocks. At the end of the test, the blocks were split, the anodic steel bars were taken out, scrubbed with wire brush, wiped with a

dry cloth and weighed to determine the mass loss caused by corrosion. The corrosion rate (mm/year) of the steel bars was calculated using the following equation:

$$\text{corrosion rate} = \frac{1000 \times m}{A \times t \times \rho} \quad \text{Eq (1)}$$

where m is the mass loss in grams, q is the density of steel of 7.87g/cm^3, A is the complete surface area of the steel attacked by corrosion in mm^2 and t is the test duration in year. To monitor the corrosion rate, the macrocell current was also determined using the Ohm's law (Eq. 2):

$$I_{macrocell} = \frac{V}{R} \quad \text{Eq (2)}$$

where $I_{macrocell}$ is macrocell current in A, V is the measured voltage between anode and cathodes in V, R is the electrical resistance between the anode and cathodes, 100 Ω. The third parameter to reflect corrosion is half-cell potential of anodic steel bars that was measured by placing a half-cell (copper electrode in saturated copper sulphate solution) on the test surface.

Pore Solution Expression and Bulk Electrical Resistivity

At the age of 90 days, cores with diameter of 60mm were cut from the 250x250x110mm concrete blocks containing no steel bars. A slice with a thickness of 10mm from the casting surface was cut off. A saturation procedure similar to that used in Section 2.4.2 was used to introduce moisture into the remaining 50mm core. The pore solution within the core was extracted by using a specialist pore fluid expression device capable of applying pressures up to 300tonnes/m^2. pH and conductivity of the pore solution were measured immediately by using a pH meter and a conductivity meter. The concentration of Na^+ and S^{2-} in the solution was analysed subsequently by using an inductively coupled plasma-optical emission mass spectrometer (ICP-MS).

RESULTS AND DISCUSSION

Slump and Compressive Strength

The slump and compressive strength of AAS and PC concretes are summarised in Table 2. As can be seen from this table, except those mixes with NaO% of 8, all mixes had a slump between 55 to 75 mm (satisfying the target slump of 40-90mm), and the slump of the AAS concretes increased with the increase of Na_2O%. This is in agreement with the results reported by Allahverdi et al. [20] and Karahan and Yakupoglu [21], who have reported the plasticising effect of Na_2O component. It seems, the Ms had no significant influence on the slump of the AAS concretes until Na_2O% was increased to 6%, beyond which the slump increased with the increase of Ms. For a given Na_2O%, an increase in Ms means an increase in the SiO_2 component, which in turn increases the viscosity. Proportionately the total liquid content in mix (for AAS concrete that is WG + NaOH + additional water) has also increased. When Na_2O% was increased, the total liquid content also increased, which resulted in an increase in the slump.

Table 2. Slump and compressive strength of the AAS and PC concretes

Mix ID (Na_2O-MS)	Slump (mm)	Compressive strength (MPa)		
		3d	28d	91d
4%-0.75	55	22.3±0.1	44.7±0.2	46.4±1.0
4%-1.00	55	21.8±0.1	46.7±1.0	55.6±0.6
4%-1.50	55	1.7±0.0	49.5±0.2	52.6±2.3
4%-2.00	55	1.4±0.0	33.3±0.4	44.1±0.1
6%-0.75	65	31.7±0.7	47.3±0.0	51.8±2.4
6%-1.00	65	37.3±0.2	53.6±0.0	59.1±0.8
6%-1.50	65	20.3±0.7	60.8±0.1	67.4±2.6
6%-2.00	75	8.0±0.0	59.6±0.2	68.7±2.1
8%-0.75	70	32.3±0.0	51.9±0.1	56.2±0.2
8%-1.00	105	32.7±2.4	53.6±0.1	67.1±0.6
8%-1.50	145	34.1±0.7	59.3±3.2	70.5±2.5
8%-2.00	180	11.7±0.2	55.4±0.2	65.0±0.8
PC	50	35.4±1.2	58.9±1.8	66.3±2.3

Note: Mixes 4%-0.75 and 4%-2.0 did not meet the required strength of 45 MPa at 28 days

The compressive strength of the concretes at the ages of 3, 28 and 91 days in Table 2 shows that not all the AAS mixes satisfied the strength class of C45. Further, the presence of the retarder had affected compressive strength development of AAS concretes, particularly at the early age. The increase of Na_2O% generally increased the compressive strength of the AAS concretes, which is in agreement with the results reported by the others due to increasing amount of C-S-H [2, 8]. The AAS concretes with Ms of 1.50 generally obtained the highest compressive strength, which agrees with the results reported previously [22]. It is noted

that the PC reference mix has a similar compressive strength to the AAS mixes with 6% Na_2O, but the water to binder ratio of AAS concretes was 0.47, higher than that of the PC concrete, which was 0.42.

Chloride Diffusivity, Electrical Resistivity and Pore Solution Characteristics

The non-steady state chloride diffusion coefficient (D_{nssd}) of the AAS concretes is compared with that of the PC concrete in Fig. 2. It can be seen that the D_{nssd} of the former was much lower than that of the PC reference despite having a higher water to binder ratio. This suggests that, in comparison to the PC concrete, the AAS concretes offered better resistance to chloride ingress. As indicated in Fig. 2, the D_{nssd} of the AAS concretes decreased with the increase of Na_2O% from 4 to 8. Al-Otaibi [23] and Karahan and Yakupoglu [21] have reported that porosity of AAS decreases with an increase of Na_2O%. Meanwhile, the hydration degree of GGBS increases with the increase of Na_2O% [4]. More hydration products would be formed in the AAS with a higher Na_2O%, which in turn would increase the binding capacity of either/both chlorides and/or their accompanying sodium cations. Both factors may have contributed to the effect of Na_2O% on D_{nssd}. It is also found in Fig. 2 that Ms around 1.50 is optimum for the hydration of AAS, which gives the reduced porosity and enhanced binding capacity of AAS, naturally leading to the lowest D_{nssd}.

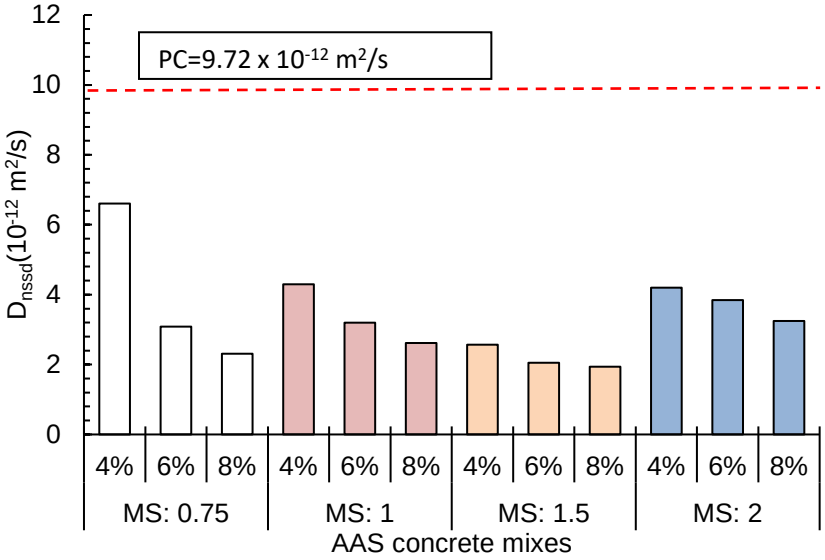

Figure 2. Non-steady state chloride diffusion coefficients of the concretes

The bulk electrical resistivity of the concretes was measured in an attempt to indicate the pore structure of concrete and to further explain the D_{nssd} results. Figure 3(a) show the results of bulk resistivity of AAS. It is clear that the resistivity of AAS concretes is much higher than that of the PC mix.

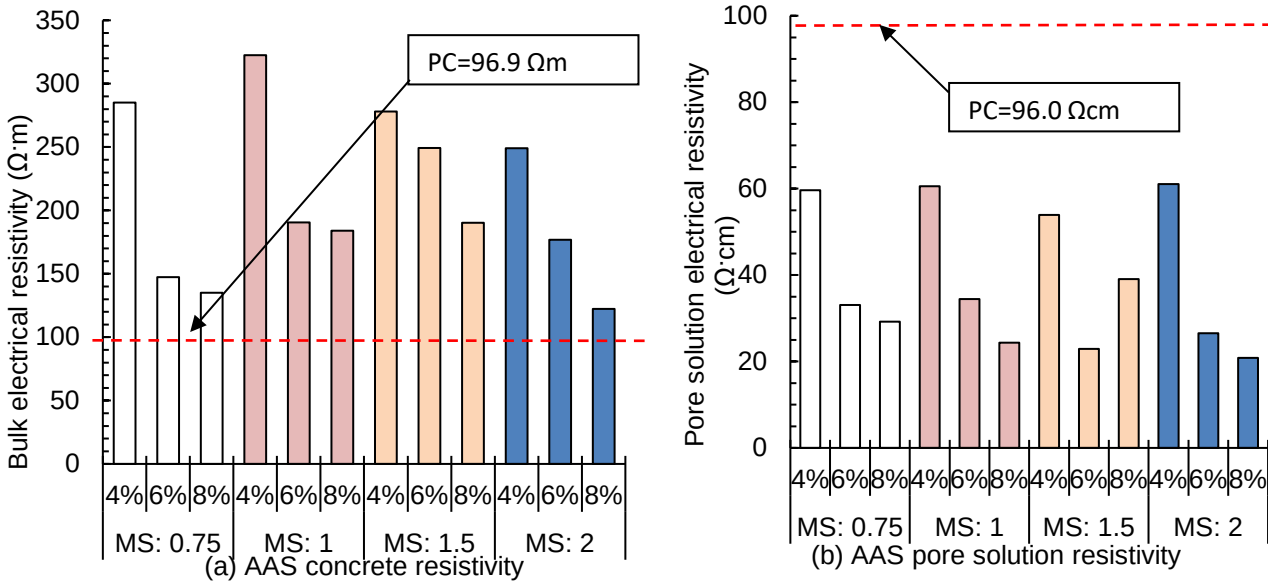

Figure 3. Bulk and pore solution electrical resistivity of AASC and PC concretes

It is known that electrical resistivity is significantly affected by the pore solution conductivity of the concrete and therefore bulk resistivity alone cannot be used to represent the pore structure of concretes [24]. Therefore, the pore solution conductivity of the concretes was also measured and its reciprocal (pore solution resistivity) is plotted in Fig. 3(b). This figure shows that the AAS concretes have lower pore solution resistivity than the PC concrete. The model proposed by Whittington et al. [25] could be used to analyse the results further; the reason for the higher bulk resistivity of the AAS concretes could be attributed to their denser tortuous pore structure and/or lower conductivity of the binder matrix. As the pore solution of AAS concretes is highly conductive, the influence of the binder matrix on the conductivity of the pore system is insignificant. Therefore, there is higher ionic flow through pore solution than the binder matrix. However, results in Fig. 3(a) would suggest that the pore structure of AAS concrete was more resistive than that of the PC concrete. This is possible only if the pore structure of the binder matrix itself is dense and tortuous and hence less conductive. As Fig. 2 shows that the AAS concretes had lower diffusivity, another contributing factor for the improved chloride resistance of the AAS concretes might be the increased binding capacity of AAS matrix, which is discussed below [6].

C-S-H (type I), C-A-S-H and hydrotalcite are the main hydration products in AAS [26] and they have much higher potential to bind alkali cations [2, 4]. Substantial amount of Na^+ is being introduced into the AAS concretes at the beginning of the mixing [4]. However, after 3 months of curing, a dramatic reduction in the concentration of free Na^+ is observed in the AAS concretes, as reported in Table 3. This would suggest that during the transport of chlorides, there is the potential for significant binding of the accompanying sodium cations by the hydrates to occur in the AAS concretes. The total chloride content at the surface of the AAS concretes is higher than that of the PC concrete, as shown in Fig. 4. Greater ionic exchanges between the exposure solution (Na^+ and Cl^-) and the available ions in AAS concrete could increase the potential binding sites. Such binding could retard the further ingress of chlorides in such concretes and reduce their chloride diffusivity, as seen in Fig. 2. The lower pH for the AAS concretes (refer to Table 3), which could be attributed to the lower sodium concentration and/or the higher sulphide concentration, could also have enhanced their chloride binding capacity due to a competition in absorption between Cl^- and OH^- [27], and hence, could further reduce the D_{nssd}.

Table 3. pH, Na^+ and S^{2-} of the pore solution of AAS concrete after 3 month of curing

Mix ID (Na_2O-MS)	pH	Na^+ (ppm)	S^{2-} (ppm)
4%-0.75	11.7	2154	2458
4%-1.00	11.9	4740	1953
4%-1.50	10.5	58.96	3786
4%-2.00	9.9	121.2	4348
6%-0.75	11.9	96.26	5661
6%-1.00	11.9	69.19	6210
6%-1.50	11.4	42.18	6245
6%-2.00	9.9	18.20	6292
8%-0.75	12.4	202.0	664.0
8%-1.00	12.2	244.0	590.0
8%-1.50	10.8	185.3	618.3
8%-2.00	11.9	64.34	608.0
PC	12.5	1234	329.6

Corrosion of the Embedded Steel

Figure 4 shows the corrosion rates of steel bar in AAS and PC concrete specimens. As shown in Fig. 4(a), the corrosion rate of the steel bars in the AAS concretes depends on the mix proportions, with some mixes showing better corrosion resistance and some others giving a higher corrosion rate in comparison to that of the PC concrete. This is an unexpected observation, because the AAS concretes in this study have better pore structure and lower chloride diffusivity, which should have given a lower corrosion rate of the embedded steel bars. Figure 4(b) shows the physical appearance of the corroded steel bars in AAS concrete (MS 1, Na_2O% 4) and PC concrete specimens at the end of the test regime. It can be seen that the steel bar in the AAS concrete corroded significantly, with most of the steel surface area covered in corrosion products along with occasional pits. The reason for relatively poor performance of the steel bars in the AAS concretes could be attributed to the outward diffusion of ions from the concrete cover into the exposure solution during the intermittent chloride ponding. Outward diffusion of alkali materials may have resulted in the reduction of the pH values in the concrete cover (see Table 3). Without the buffering of $Ca(OH)_2$ in the AAS concretes, the continuous diffusion could have resulted in the dissolution of the binder from the cover concrete. Furthermore, carbonation may have occurred during the drying period, which could also have resulted in the disintegration of the binder of the concrete cover. This is particularly important for AAS concrete [23]. Nevertheless, it should be noted that intermittent chloride ponding in this study could have enhanced capillary absorption and therefore the transport is not entirely diffusion based. Steel was located 15 mm from the chloride ponding surface in this

study. This would mean that steel was located in a region that would have been influenced by the outward diffusion and therefore pH of surrounding concrete was low. All of these could have contributed to the increased rate of corrosion. Therefore, it is important to investigate thoroughly the corrosion resistance of AAS concretes for different exposure conditions before general conclusions on their resistance to chloride induced corrosion is made.

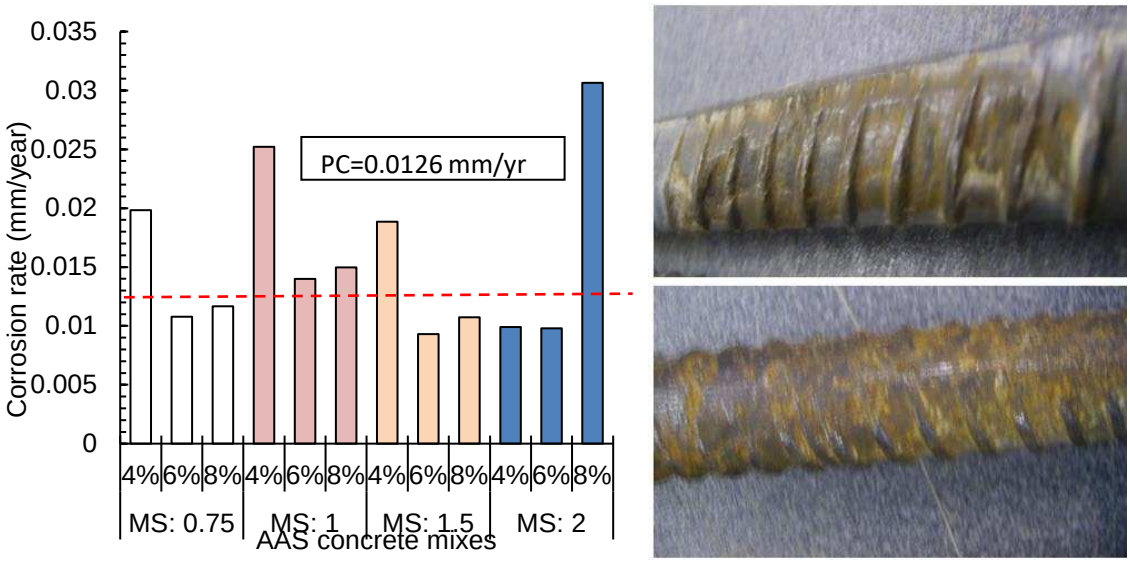

(a) Corrosion rate (b) Corrosion of the anodic steel bar

Figure 4. Corrosion rates calculated from the gravimetric mass loss of steel and corrosion of anodic steel bars at the end of the exposure regime

Figure 5 plots corrosion rates against different influencing factors. In Fig. 5(a) and (b), there is no relationship between the rate of corrosion and both the chloride diffusivity and the bulk resistivity of AAS concretes. This is considered to be due to any of the following two reasons: (i) in addition to chloride diffusivity and bulk resistivity, corrosion rate of the embedded steel in concrete is also dependent on the free chloride concentration, pH, availability of oxygen and water, and concentration of sulphides in the pore solution of the concrete; and (ii) absorption occurs in the intermittent chloride ponding regime, which is not the case for the immersion test and consequently the chloride transport in these two cases is different. From Fig. 5(c) and (d), it can be seen that there is a fairly good correlation between the corrosion rate of steel and the concentration of sulphides (S^{2-}) and Na^{+} in the pore solution for the concretes studied. As expected [8], the corrosion rate generally decreased with the increase of the concentration of sulphides. Presence of sulphides in pore solution of concrete can significantly reduce the redox potential of the pore solution. Redox potential measurement is a reflection of oxidation and reduction activities. The reduction of the redox potential is a result of the increase of reduction atmosphere, which would protect the embedded steel from its oxidation to a certain extent to reduce the corrosion rate of the steel. The concentration of Na^{+} also strongly affects the corrosion rate, more Na^{+} the faster the corrosion.

Figures 6(a) and 6(b) respectively shows the measured half-cell potentials and galvanic corrosion data for PC concretes. It can be found from these figures that corrosion of the steel in the PC concrete was not initiated during the first 50 days, indicated by less negative half-cell potentials than -200mV (less than 10% probability of corrosion, according to ASTM C876) and low values of galvanic corrosion (corrosion current density less than 0.1 $\mu A/cm^2$, corresponding to phase I). However, between 50 days and 90 days, the half-cell values became more negative (-200 to -350 mV, indicative of 50% probability of corrosion), with associated increase in galvanic corrosion, but still the corrosion current density less than 0.1 $\mu A/cm^2$. Beyond 90 days up to 250 days, the half-cell potentials became more negative than -350 mV, indicative of more than 90% probability of corrosion (phase II), with corresponding increase in corrosion current density to 0.5 $\mu A/cm^2$(phase II). Although some measured current density values during this period was greater than 0.5 $\mu A/cm^2$ on an average it can be considered that the degree of corrosion represented phase II. That is, a strong correspondence between the half-cell potentials and the macrocell corrosion current was found for the PC concrete.

Figures 7(a) and 7(b) show the half-cell potentials and galvanic corrosion measurements for a typical AAS concrete. Here, the link between half-cell potentials and corrosion current density is weak. More specifically, the half-cell potentials would suggest that there was greater than 50% probability of corrosion from an early age, but the corrosion current remained at a value around 0.1 $\mu A/cm^2$. In Fig. 8, the half-cell potentials are plotted against the corrosion current density for all of the concretes. Clearly, there is no obvious trend

between the two parameters, highlighting that there are limitations in using either the half-cell potentials or the galvanic current measurement, or both, for assessing the onset and rate of corrosion of steel in AAS concretes.

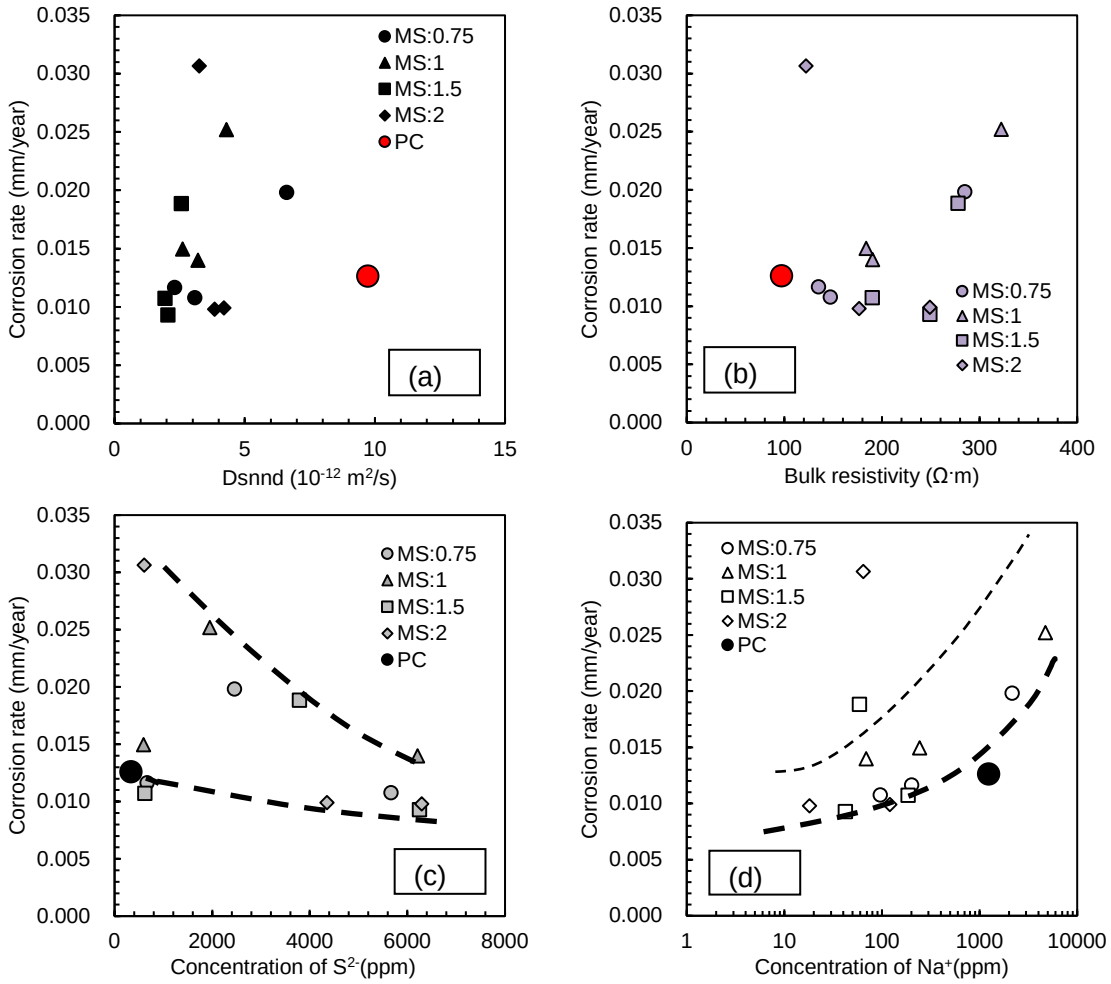

Figure 5. Relationship between corrosion rate and different contributing factors

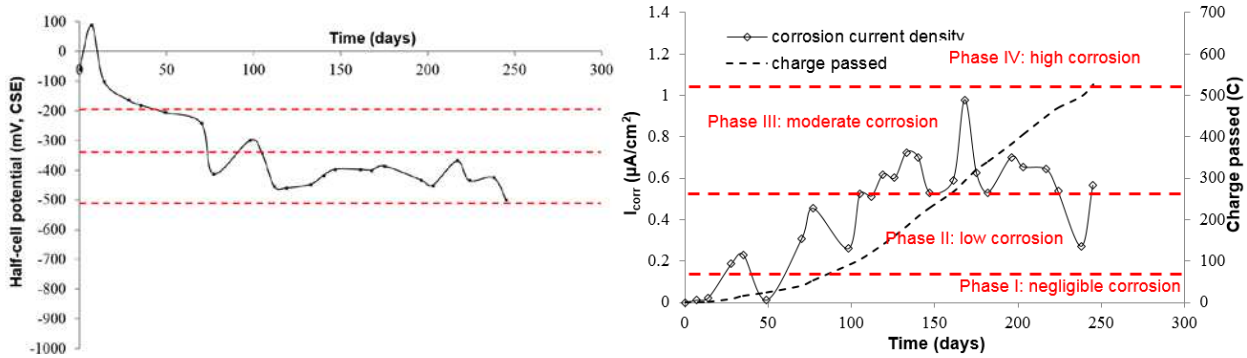

(a) Half-cell potentials for PC (b) Galvanic corrosion data for PC

Figure 6. Trend of half-cell potentials and galvanic corrosion data for PC concrete

Whilst discussing Fig. 4, it has already been established that there was the rapid loss of the passivating film in AAS samples, which were attributed to two reasons. Firstly, the low alkalinity of the pore solution of AAS concretes (Table 3) directly affects the stability of the passivating film. Secondly, the higher sulphide concentration in AAS concretes can be adsorbed on to the steel surface and accelerate the break down rate of the passivating film. However, despite the rapid corrosion initiation in AAS concretes, the corrosion current of the steel in AAS concrete is much lower than that in PC. This could be due to the lesser amount of Cl^- content around the steel bar and the denser microstructure of the AAS concretes (both of which can be assigned to the lower chloride diffusivity shown in Figure 2). In addition, the high sulphide concentration in AAS concrete can protect the steel from oxidation and reduce the rate of corrosion. These results suggest that the

corrosion rate of steel in AAS concrete needs to be assessed by a multi-parameter approach and general correlation established for the PC system may not be valid for this binding system.

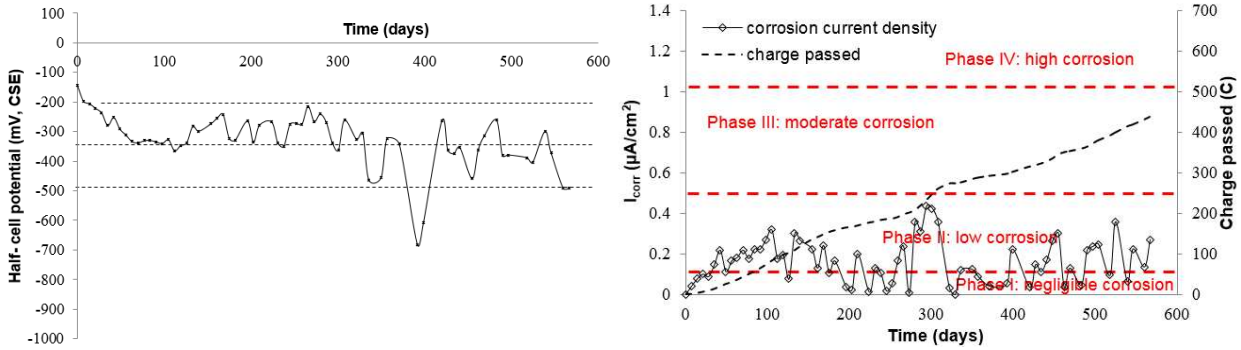

(a) Half-cell potentials for AASC (b) Galvanic corrosion data for AASC (AASC: Na_2O%: 6, Ms: 5.0)

Figure 7. Trend of half-cell potentials and galvanic corrosion data for a typical AAS concrete

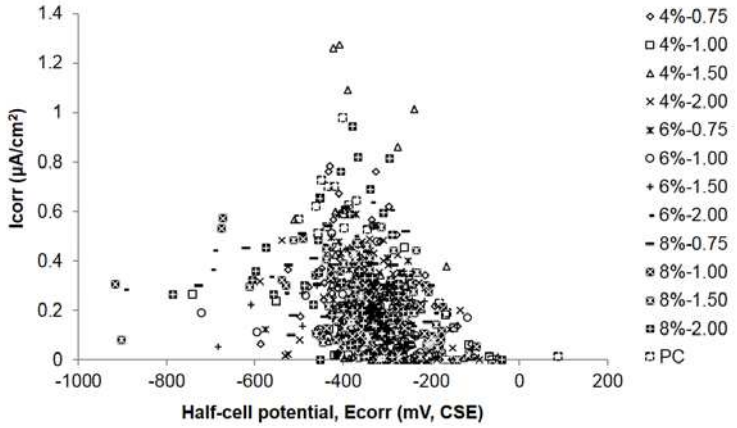

Figure 8. Relationship between half-cell potentials and galvanic corrosion for AAS concretes

SUITABILITY OF MIXES FOR CHLORIDE EXPOSURE REGIMES IN EN 206-1

Table 4 gives the summary of the non-steady state diffusion coefficient and the rate of corrosion measured for both the PC and AAS concretes. The pH, sulphide content, 28-day compressive strength and slump are also presented in this table. As can be seen from this table, compared to the PC, all AAS concretes had a lower chloride diffusivity, but there was no corresponding decrease in rate of corrosion in all AAS concretes. The mixes which do not satisfy the various assessment criteria in this table are highlighted, which show that amongst the 12 AAS mixes studied, only the combination of 6% Na_2O-0.75 MS, 6% Na_2O-1.50 MS, 6% Na_2O-2.00 MS and 8% Na_2O-0.75 MS are suitable for the XS2, XS3 and XD3 exposure classes in EN 206-1. This would suggest that chloride diffusivity alone is not sufficient to qualify AAS concretes against chloride induced corrosion, but other parameters as discussed earlier need to be given emphasis.

Table 4. Rate of corrosion (mm/yr) of the AAS concretes and the PC concrete

Mix ID (Na_2O-MS)	D_{nnsd} (x 10^{-12} m^2/s)	Rate of Corrosion (mm/yr)	pH (<11 highlighted)	S^{2-} (ppm)	Compressive Strength (MPa)	Slump (mm)
4%-0.75	6.59	0.020	11.7	2458	44.7±0.2	55
4%-1.00	4.25	0.025	11.9	1953	46.7±1.0	55
4%-1.50	2.54	0.019	10.5	3786	49.5±0.2	55
4%-2.00	4.14	0.010	9.9	4348	33.3±0.4	55
6%-0.75	3.07	0.011	11.9	5661	47.3±0.0	65
6%-1.00	3.18	0.014	11.9	6210	53.6±0.0	65
6%-1.50	2.01	0.009	11.4	6245	60.8±0.1	65
6%-2.00	3.76	0.010	9.9	6292	59.6±0.2	75
8%-0.75	2.24	0.012	12.4	664.0	51.9±0.1	70
8%-1.00	2.58	0.015	12.2	590.0	53.6±0.1	105
8%-1.50	1.88	0.011	10.8	618.3	59.3±3.2	145
8%-2.00	3.26	0.030	11.9	608.0	55.4±0.2	180
PC	**9.70**	**0.012**	**12.5**	**329.6**	**58.9±1.8**	**50**

Note: Red colour text shows mixes which do not satisfy the assessment criterion

CONCLUSIONS

On the basis of results discussed in this paper, the following conclusions have been drawn:

1) Compared to the PC concrete, the AAS concretes achieved lower non-steady state diffusion coefficient, but there existed interactions between both Na_2O % and Ms of water glass which need to be taken into account in any service life models using chloride diffusivity as the input parameter.
2) The lower chloride diffusivity was accompanied by higher bulk electrical resistivity of AAS concretes, but not in all cases by lower rate of corrosion.
3) The corrosion rate of the steel bars in the AAS concretes depended on a number of factors, including the concentration of sodium and the molar ratio of the water glass used as the activator.
4) It is important to ensure that there is no outward leaching of alkalis for AAS concretes to perform well in chloride exposure environments.

ACKNOWLEDGEMENT

The experiments described in this paper were carried out in the concrete laboratory of Queen's University Belfast, which is gratefully acknowledged. The supports from Kunming University of Science and Technology, University College London, Chongqing University and University of Leeds during the preparation of this paper are highly appreciated. The authors gratefully acknowledge discussions with Prof John Provis of University of Sheffield (UK) and the financial support provided by EPSRC (UK), NSFC (China), the Open Research Funds for the Shenzhen University (China) and State Key Laboratory of High Performance Civil Engineering Materials (China).

REFERENCES

1. Shi C, Wu X and Tang M (1993), Research on alkali-activated cementitious systems in China: a review, Advances in Cement Research, 5(17), 1-7.
2. Shi C, Krivenko PV and Roy D (2006), Alkali-activated cements and concretes, Taylor & Francis, London.
3. Ismail I, Bernal SA, Provis JL, San Nicolas R, Brice DG, Kilcullen AR, Hamdan S and van Deventer JSJ (2013), Influence of fly ash on the water and chloride permeability of alkali-activated slag mortars and concretes, Construction Building Materials 48: 1187–1201.
4. Puertas F, Fernandez-Jimenez A and Blanco-Varela MT (2004), Pore solution in alkali-activated slag cement pastes, Relation to the composition and structure of calcium silicate hydrate, Cement Concrete Research 34:139–148.
5. Holloway M and Sykes JM (2005), Studies of the corrosion of mild steel in alkali-activated slag cement mortars with sodium chloride admixtures by a galvanostatic pulse method, Corrosion Science 47(12):3097–3110.
6. Provis JL, Myers RJ, White CE, Rose V and van Deventer JSJ (2012), X-ray microtomography shows pore structure and tortuosity in alkali-activated binders, Cement Concrete Research 42: 855–864.
7. Ma QM, Nanukuttan S, Basheer PAM, Bai Y and Yang CH (2016), Chloride transport and the resulting corrosion of steel bars in alkali activated slag concretes, Materials and Structures 49: 3663-3677.
8. Criado M, Bernal SA, Garcia-Trinanes P and Provis JL (2018), Influence of slag composition on the stability of steel in alkali-activated cementitious materials, Journal of Materials Science 53(7): 5016-5035.
9. Broomfield, J (2007), Corrosion of steel in concrete: Understanding, Investigation and Repair, 2nd Edition, Taylor and Francis, London.
10. BS EN 206-1 (2000), Concrete. Specification, performance, production and conformity, BSI, London
11. BS EN 15167-1 (2006), Ground granulated blast furnace slag for use in concrete, mortar and grout—Part 1 Definitions, specifications and conformity criteria, BSI, London.
12. Yang C and Pu X (1993), Retarder of alkali activated slag, Chinese patent, 91108316.2.
13. BS EN 197-1 (2000), Cement—Part 1: Composition, specifications and conformity criteria for common cements, BSI, London.
14. BS 1881-125 (1986), Testing concrete —Part 125: Methods for mixing and sampling fresh concrete in the laboratory, BSI, London.
15. BS EN 12350-2 (2009), Testing fresh concrete Part 2: Slump-test, BSI, London.
16. BS EN 12350-3 (2009), Testing hardened concrete Part 3: Compressive strength of test specimens, BSI, London.
17. NT BUILD 443 (1995), Concrete, hardened: accelerated chloride penetration.
18. NT BUILD 492 (1999), Concrete, mortar and cement-based repair materials: chloride migration coefficient from nonsteady-state migration experiments.

19. Tang L (2005), Guideline for practical use of methods for testing the resistance of concrete to chloride ingress, Chlortest Report, European Commission, Brussels.
20. Allahverdi A, Shaverdi B and Najafi KE (2010), Influence of sodium oxide on properties of fresh and hardened paste of alkali-activated blast-furnace slag, International Journal of Civil Engineering 8(4):304–314.
21. Karahan O and Yakupoglu A (2011), Resistance of alkali-activated slag mortar to abrasion and fire, Advance Cement Research 23(6):289–297.
22. Krizan D and Zivanovic B (2002), Effects of dosage and modulus of water glass on early hydration of alkali-slag cements, Cement Concrete Research 32(8):1181–1188.
23. Al-Otaibi S (2008), Durability of concrete incorporating GGBS activated by water-glass, Constr Build Mater 22(10):2059–2067.
24. Basheer PAM, Gilleece PRV, Long AE and McCarter WJ (2002), Monitoring electrical resistance of concretes containing alternative cementitious materials to assess their resistance to chloride penetration, Cement Concrete Composites 24(5):437–449.
25. Whittington HW, McCarter J and Forde MC (1981), The conduction of electricity through concrete, Magazine Concrete Research 33(114):48–60.
26. Wang SD and Scrivener KL (1995), Hydration products of alkali activated slag cement, Cement and Concrete Research 25: 561-571.
27. Tritthart J (1989), Chloride binding in cement II, The influence of the hydroxide concentration in the pore solution of hardened cement paste on chloride binding, Cement Concrete Research 19:683–691.